22 Nov 2021

Machine Learning Identifies Liquids Employing a Simple Fiber-Optic Tip Sensor

Wassana Naku

Chen Zhu

Anand K. Nambisan

Rex E. Gerald

et. al. For a complete list of authors, see https://scholarsmine.mst.edu/ele_comeng_facwork/4447

Recommended Citation

W. Naku et al., "Machine Learning Identifies Liquids Employing a Simple Fiber-Optic Tip Sensor," *Optics Express*, vol. 29, no. 24, pp. 40000-40014, Optica Publishing Group, Nov 2021.
The definitive version is available at https://doi.org/10.1364/OE.441144

Research Article | Vol. 29, No. 24 / 22 Nov 2021 / Optics Express 40000
Optics EXPRESS

Machine learning identifies liquids employing a simple fiber-optic tip sensor

WASSANA NAKU,[1,2] CHEN ZHU,[1,2,3] ANAND K. NAMBISAN,[1] REX E. GERALD II,[1] AND JIE HUANG[1,4]

[1]Department of Electrical and Computer Engineering, Missouri University of Science and Technology, Rolla, MO 65401, USA
[2]These authors contributed equally to this work
[3]cznwq@mst.edu
[4]jieh@mst.edu

Abstract: We proposed an extremely simple fiber-optic tip sensor system to identify liquids by combining their corresponding droplet evaporation events with analyses using machine learning techniques. Pendant liquid droplets were suspended from the cleaved endface of a single-mode fiber during the experiment. The optical fiber-droplet interface and the droplet-air interface served as two partial reflectors of an extrinsic Fabry-Perot interferometer (EFPI) with a liquid droplet cavity. As the liquid pendant droplet evaporated, its length diminished. A light source can be used to observe the effective change in the net reflectivity of the optical fiber sensor system by observing the resulting optical interference phenomenon of the reflected waves. Using a single-wavelength probing light source, the entire evaporation event of the liquid droplet was precisely captured. The measured time transient response from the fiber-optic tip sensor to an evaporation event of a liquid droplet of interest was then transformed into image data using a continuous wavelet transform. The obtained image data was used to fine-tune pre-trained convolution neural networks (CNNs) for the given task. The results demonstrated that machine learning-based classification methods achieved greater than 98% accuracy in classifying different liquids based on their corresponding droplet evaporation processes, measured by the fiber-optic tip sensor.

1. Introduction

The evaporation process of liquids involves molecules transitioning from a liquid to a gas phase when there is sufficient thermal activation energy [1]. Liquid droplets have many properties which are studied, such as geometry, formation, and evaporation. These properties are affected by various factors, for example, viscosity, surface tension, and the chemical composition of the liquid [2]. A droplet is usually classified as either pendant or sessile based on the orientation of the surface on which it is formed. A pendant nonmoving droplet is formed when the droplet is suspended on a surface facing the ground, while a sessile droplet is formed when the droplet rests on an upward-facing surface. Studying droplet evaporation is important for many applications, such as the development of monolayers [3], inkjet printing [4], and the drawing of nanofibers [5]. Many state-of-the-art instruments, such as optical microscopes, confocal microscopes [6], and infrared spectrometers [7], have been used to observe the droplet evaporation phenomenon and to understand particle and film deposition on solid substrates. Real-time measurements of droplet evaporation events are also used in the medical analysis of tears to identify patients with gland dysfunctions [8].

Optical fiber sensors have been widely used in many areas such as civil infrastructure [9,10], chemical synthesis plants, and biomedical industries [11] for measuring various physical and chemical parameters such as strain, displacement, curvature, temperature, gas concentration, and liquid level [10,12–15]. Optical fiber sensors have many advantages compared to conventional

#441144 https://doi.org/10.1364/OE.441144
Journal © 2021 Received 22 Aug 2021; revised 18 Oct 2021; accepted 31 Oct 2021; published 16 Nov 2021

Optics EXPRESS

electronic sensor devices, including high accuracy, lightweight, the capability of distributed sensing, immunity to electromagnetic interference, small size, and robustness in harsh environments [16–18]. Currently, there are many types of optical fiber sensor configurations, such as fiber grating sensors [19], fiber optic gyroscopes [20], and interferometer sensors [21], etc. Particularly, fiber optic sensors are also employed in the analysis of liquid droplets, as seen in [22–24]. One of the most broadly used configurations in the field of liquid droplet analysis is the extrinsic Fabry-Perot interferometer (EFPI)-based sensor because it is simple and highly sensitive [13,25,26]. Using the EFPI technique for studying evaporation events of liquids was previously reported in the literature, and more information can be found in [27–29]. Dual-mode fiber laser microcavities have also been used for real-time gas mixture detection by solving a set of linear equations [30]. However, these papers only performed analyses of the evaporation dynamics and did not use the data for liquid identification, while some used simple models for performing classification, which our model improves upon significantly.

Deep learning methods are a subset of machine learning techniques, which imitate the structure and function of human learning processes. In practice, deep learning methods are used to extract features from data and subsequently transform the data into different levels of abstraction. Also, convolution neural networks (CNNs) are specialized types of machine learning models inspired by the function of the human eye and are primarily used for processing image data [31]. Both deep learning and convolutional neural network models are widely used in image processing and computer vision applications, such as feature extraction and image classification. An example of such an application is heartbeat classification from electrocardiogram (ECG) waveforms [32]. Machine learning techniques have been adopted in various areas of research, such as in medicine [33], seismology [34], and remote sensing [35]. In recent years, motivated by their successful application in many scientific and engineering fields, machine learning techniques have been combined with advanced fiber-optic sensing technologies for producing a new generation of smart and intelligent sensing systems and networks. Examples include using machine learning techniques to analyze data acquired from distributed fiber-optic acoustic sensors for event identification and leakage detection [36]. Deep learning techniques have also been used in finding key parameters for Kerr comb spectra using measured spectral transmissions in microcavities [37]. Another interesting application of machine learning techniques was the transformation of a one-dimensional fiber-optic inclinometer into a sensor device that can sense blunt-force impact events in three-dimensional space [38].

In this study, we proposed and demonstrated a simple yet intelligent sensing system for the identification of liquids. The sensing system includes an extremely simple fiber-optic tip sensor, which is a cleaved single-mode optical fiber, and a data acquisition unit. By immersing the fiber-tip sensor into and subsequently pulling the sensor out of the liquid of interest, a pendant droplet of liquid is formed on the cleaved endface of the optical fiber. More importantly, the liquid droplet forms an EFPI, whose effective reflectance is a function of the length of the liquid droplet. As a result, when probed using single-wavelength light, the effective reflectance of the sensor changes quasi-periodically as the liquid evaporates from the fiber endface. A time transient response corresponding to the evaporation event of the pendant liquid droplet is recorded and considered as a fingerprint of the particular liquid under test. A large amount of data was acquired for different types of liquids for this purpose. Continuous wavelet transforms were used to convert the two-dimensional time transient responses to image data, which were used as the input to train, validate, and test CNN models. The results show that the CNN models employed in this work effectively identify different liquids based on their evaporation fingerprints measured by the simple fiber-optic tip sensor.

Optics EXPRESS

2. Sensor design and measurement principle

2.1. Experiment setup and sensor design

The experiment setup, including an illustration of a pendant droplet cavity, for employing an EFPI-based sensor for liquid droplet evaporation studies are schematically shown in Fig. 1. For the signal interrogation system, a high-speed photodetector (PD, Nirvana Detector, Model 2017) and a PC Oscilloscope (PicoScope 4642, Pico Technology) were employed. A tunable laser source (TLS, Hewlett-Packard 8168F) was used as the light source. The sensing element was a single-mode fiber (SMF). First, we stripped the coating to expose a section of bare fiber near the two ends of the fiber, and then we cleaved both ends of the bare fiber. One of the endfaces was connected to a fiber-optic circulator, and the other cleaved endface was used as the head of the liquid droplet evaporation sensor. The output wavelength of the tunable laser source was set to 1550 nm with a power level of 0 dBm. Light from the tunable laser source was launched into Port 1 of the fiber optic circulator (FOC) and then directed to the sensor head. The signal reflected from the sensor head returned to Port 2 of the FOC and was redirected to the photodetector via Port 3. A computer connected to the oscilloscope was used to record the time-domain signal derived from the liquid cavity modulated by evaporation. A schematic representation of the setup can be seen in Fig. 1(a). In Fig. 1(b) we show the reflections caused due to the liquid droplet at the fiber endface, one at the fiber-liquid interface, and the second at the liquid-air interface. Both reflectors form a low-finesse Fabry-Perot interferometer cavity. In the experiment, the fiber tip (i.e., the sensor head) is manually and carefully dipped into the test solvent in a vertical direction and subsequently pulled out from the solvent, resulting in the formation of a liquid droplet at the surface of the cleaved optical fiber endface. The pendant liquid droplet formed on the fiber endface can be considered as a thin film cavity that forms the EFPI.

The light intensity reflected by the EFPI can be formulated as [39]

$$I = I_1 + I_2 + 2\sqrt{I_1 I_2}\cos\left(\frac{4\pi nd}{\lambda} + \varphi\right) \tag{1}$$

where I_1 and I_2 are the intensity of light reflected by the fiber-liquid interface and the liquid-air interface, respectively; n is the refractive index of the liquid; d is the cavity length, i.e., the length of the pendant droplet; φ is the initial phase difference between the two interfering reflected waves; and, λ is the wavelength of the incident light. Therefore, for a probing light of a fixed wavelength, the reflected intensity is directly dependent on the length of the pendant droplet. As the droplet evaporates, the length of the droplet gradually decreases, leading to quasi-periodic changes of the reflected light intensity based on Eq. (1). The reflected intensity is converted into an electrical signal via the oscilloscope, and the corresponding electrical signal is monitored as a function of time. For each of the droplet evaporation events, a corresponding time transient signal was recorded and then further processed for use in building liquid identification models.

2.2. Data processing and machine learning

Instead of carefully calculating the evaporation rate of the liquid droplet based on the measured time transient signal for liquid identification, we proposed to use machine learning to directly map the transient signal to the type of liquid. Since the measured time transient signal is affected by the physical properties of the liquid as it undergoes evaporation it, therefore, provides very rich information about the evaporation process, and our application leverages this information for liquid identification. In our application, we use CNNs - which are currently one of the most widely used deep learning architectures - for solvent identification. In a typical CNN, a series of convolution and pooling operations are used to reduce the number of parameters required to process spatial data, e.g., images. Using traditional neural network architectures, e.g., a Multi-Layer-Perceptron (MLP), requires a much larger number of parameters that have to be

Optics EXPRESS

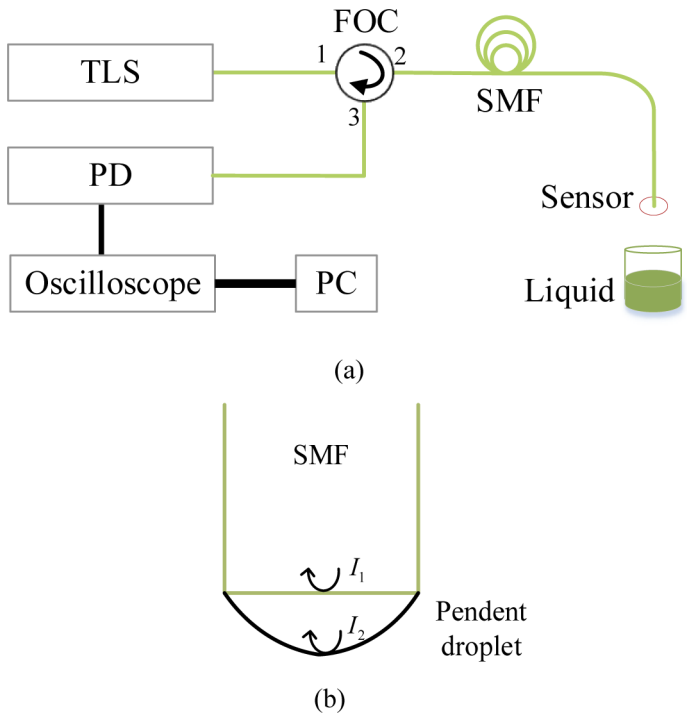

Fig. 1. Schematic of the experiment setup, including an illustration of a pendant droplet cavity forming an EFPI-based sensor device for liquid evaporation studies. (a) The schematic diagram of the experimental setup for studying the evaporation of a liquid droplet. (b) A schematic illustration of a pendant droplet on the cleaved endface of an SMF. TLS: Tunable laser source; PD: Photodetector; FOC: Fiber optic circular; SMF: Single-mode fiber; PC: Personal computer; I_1 and I_2 : Intensities from first and second EFPI reflectors, respectively.

optimized for the given task, and the extracted features are not translation-invariant [40]. In contrast, CNNs have been shown to perform extremely well in image classification tasks [41].

The first step of our workflow involved data collection and pre-processing stages. As discussed in previous sections, in the data collection stage, the EFPI sensing mechanism was used to generate a time transient signal for a droplet evaporation event for each liquid of interest; multiple signals were recorded for each liquid. Each of these signals was annotated with the name of the actual liquid. In the pre-processing data stage, we heuristically removed extraneous portions of the signal to reduce the number of sample points in each collected signal. Next, continuous wavelet transform (CWT) was utilized to calculate the CWT coefficients of each signal. Subsequently, we generated time-frequency representations of the signals called scalograms from the coefficients. The scalograms were generated by taking the absolute value of the CWT coefficients. The scalograms are similar to spectrograms, which are time-frequency representations of the signals. Spectrograms are a 3-dimensional representation of the change in signal intensity across both time and frequency. We can construct a spectrogram by essentially doing a short-time Fourier transform (STFT) over the signal. When we do the STFT, the window sizes are fixed; this is akin to using a microscope of fixed magnification (window size) to observe objects ranging from ants (low frequencies-which may need big window sizes to be captured) to viruses (high frequencies-which may only need a short window to be captured properly). However, the scalograms provided better scaling of time-vs-frequency resolution across the whole range of desired frequencies so that frequency components were better localized with respect to time [42,43]. This localization is

Optics EXPRESS

because the scalogram uses wavelets that scale the windows according to the frequency range of interest. We converted the scalograms to RGB images and resized them so that they concur with the required input size for the pre-trained CNNs we intended to use. The resized scalogram images were then used as inputs to fine-tune the pre-trained CNN. The scalograms were constructed using Morse wavelets with the symmetry parameter (γ) set to 3 and time-bandwidth product (P^2) set to 60. Morse wavelets are a flexible class of wavelets that are applicable to a wide variety of tasks [44]. For the pre-trained CNNs we use the versions of the models provided in MATLABs Deep Learning Toolbox. These models come with weights from having been trained on the ImageNet dataset for Visual object recognition. We then remove the fully connected final classification layer from these models and replace them with a new untrained fully connected final classification layer, which will learn only from our data. We do this by ensuring that the final layer accepts the same number of inputs as the old layer but with as many number of outputs as liquids to be identified for our task. This is done primarily because the initial layers of the CNNs learn more general features and behave like edge-detectors or texture detectors (this is what we desire to keep and fine-tune further on our data) while the later layers extract abstract features more geared towards the task being trained on. The final output is then passed to a SoftMax layer to generate the final scores for identification. The equation for the SoftMax layer is shown below.

$$\hat{y}_i = \frac{\exp(o_i)}{\sum_{j=1}^{K} \exp(o_j)} \tag{2}$$

where o_i is the output from the fully connected layer, which corresponds to the i^{th} liquid, and $\hat{y}_i$ is the final score for the input scalograms membership to the i^{th} liquid in the task. During training, these scores are used to optimize a Cross-Entropy loss function, and during the testing phase, we use the scores to identify the liquid. The Cross-Entropy loss function is calculated as

$$CELoss = \sum_{m=1}^{N} \sum_{n=1}^{K} y_{mn} \ln(\hat{y}_{mn}) \tag{3}$$

where N is the number of scalogram images in the training dataset, K is the number of liquids in the identification task, y_{mn} is an indicator function, which is one if the m^{th} signal is of class n and zero otherwise, and $\hat{y}_{mn}$ is the score of the model for the m^{th} input towards class n. During the test phase, the highest class score is used for identifying the liquid for the given input scalogram. The complete workflow for the process is shown in Fig. 2.

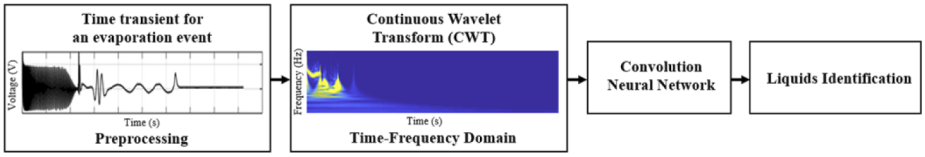

Fig. 2. Workflow schematic employing CNN for liquid classification (identification) based on the evaporation time transient.

3. Experiment results and discussion

3.1. Evaporation events of liquids

The principle aim of this paper was to classify pendant droplet evaporation events for liquids using a simple fiber optic tip sensor device and analyses by a convolution neural network (CNN). We first selected seven different types of pure liquids for our experiments, including decane,

Optics EXPRESS

milli-Q water, 2-propanol, ethanol, acetonitrile, methanol, and acetone. Some important physical properties of these liquids are included in Table 1. We initiated the experiments by first recording the droplet evaporation event signals for the seven different pure liquids using the EFPI sensor system. Figure 3 shows examples of the measured time-domain responses for the seven liquids within a period of twelve seconds obtained from the EFPI sensor system. Differences in the EFPI experiment time-domain transients can easily be observed between the different pure liquids. The most evident differences are the time durations of droplet evaporations since different liquids have different vapor pressures and concomitant evaporation rates for identical droplet sizes and shapes. Instead of calculating the evaporation rate based on the time transient signal, temperature, droplet shape, and droplet size, we proposed using machine learning to categorize and identify the recorded signals. While it is challenging to unambiguously correlate the measured time-domain signals to the seven different pure liquids through visual inspection, a deep learning model can be used as a powerful nonlinear function approximator that can be trained to identify each liquid. In fact, the measured time transient signal for a droplet evaporation event includes rich information, such as the refractive index and the evaporation rate, thanks to the high sensitivity of the EFPI sensor system. Liquid analyses based on calculating the droplet evaporation rate from the time transient curve will unavoidably lose a portion of information [28,45]. Therefore, it is necessary to use a more advanced data-driven approach, machine learning, which can directly learn the relevant features embedded in the signal and achieve one-to-one mapping between the time transient droplet evaporation signal and the liquid identity. In this work, we will not attempt to explain the complicated processes involved in the evaporation of droplets of the liquids used in the EFPI system since there are a diverse array of variables that contribute to the measured evaporation plot [46]. Instead, we propose that machine learning can help extract features in the measured droplet evaporation plots, which can be exploited to classify (identify) the different liquids. Typically, a large and diverse composite dataset is required to train a CNN model, and the data collection is time-consuming and somewhat expensive. A more practical approach is to simply deploy a pre-trained model, trained on a bigger dataset towards some general image recognition task, and then continuously fine-tune the model with newly collected data of interest for the specific task (a so-called transfer learning process). In this work, the transfer learning process-based motif was adopted, and different models that were pre-trained on ImageNet were utilized [47].

Table 1. The physical properties of seven liquids examined in the present work.

Liquids	Formula	Molar Mass (g/mol)	Boiling Point (°F)	Vapor Pressure at 25°C (mmHg)	Density (kg/m^3)	Refractive Index
Decane	$C_{10}H_{22}$	142.29	345.4	1.43	730	1.412
Milli-Q Water	H_2O	18.02	212	23.6864	998.2	1.333
2-Propanol	C_3H_8O	60.1	180.5	43.6451	786	1.377
Ethanol	C_2H_5OH	46.07	173.1	58.7538	789	1.361
Acetonitrile	C_2H_3N	41.05	179.6	91.1898	786	1.344
Methanol	CH_3OH	32.04	148.5	126.874	792	1.329
Acetone	C_3H_6O	58.08	132.8	229.469	784	1.359

One hundred transient responses were recorded for each of the seven pure liquids. Thus, a total of 700 transient response signals were obtained from the seven different pure liquids. Next, we applied a continuous wavelet transform (CWT) to each time-domain response to convert the time-domain signal to a time-frequency representation of the signal, which we refer to as a

Optics EXPRESS

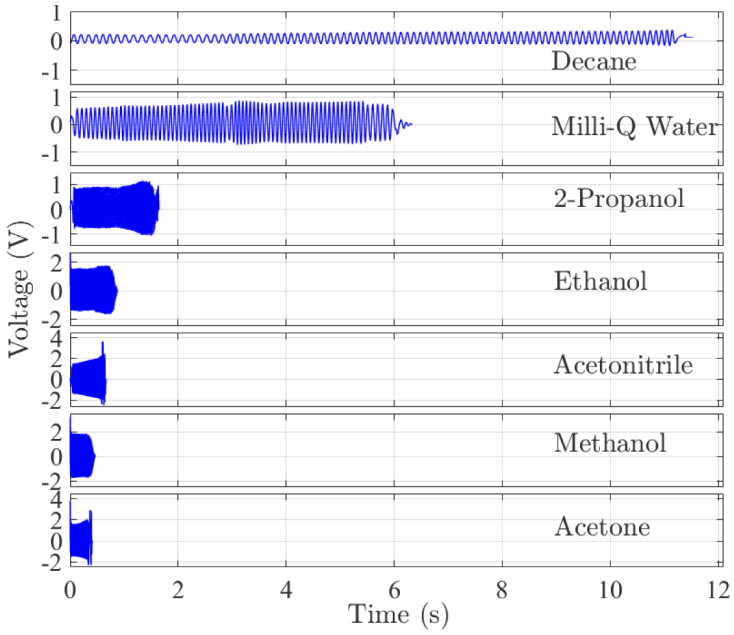

Fig. 3. Exemplary time transient signals for evaporating droplets from seven different liquids employing the EFPI sensor. Each of the transient signals corresponds to a complete evaporation event of a single droplet of liquid. For the purpose of comparison, the x-axis is set to a time period of 12s, which is the duration of the longest transient (decane).

scalogram. Figure 4 illustrates representative semi-log scalograms for the corresponding seven time-domain responses shown in Fig. 3.

The scalograms are matrices of size 169×128700, the elements of which we scale to the range 0–1. To convert these into the final images, they are then further scaled and quantized to the range 0–255 and finally converted to a pseudocolor (contour) plot. This contour plot is then resized to the desired image sizes 224×224×3 or 227×227×3, depending on the input layer of the model used. For training our models, we used the Deep Learning Toolbox in MATLAB 2018b, installed on a PC running Windows 10 with 8GB of RAM. In our work, we used five different models for training the data samples obtained from the experiments. The composite training dataset consisted of 50% of the total data samples, and the remaining 50% were split equally between the validation and test sets. We set the learning rate to a constant 0.0001 with a batch size of 32. The optimizer used to train was the ADAM optimizer [48,49]. To avoid overfitting, we trained for only five epochs. We introduced early-stopping based on the average validation loss (calculated on the entire validation set) with early-stopping patience of 3 iterations. This choice was based on the fact that previous experiments showed that the training converges very rapidly. In Fig. 5, we show the confusion matrix for the classification results from one of our models - ResNet-18 - on the composite dataset of pure liquid data samples (700 signals). The confusion matrix indicates the number of correct and incorrect class predictions for the given dataset using our model: the columns correspond to the true classes for data points in the dataset. The rows show the classes that were predicted by the network. The diagonal elements of the matrix show the number of data samples that were correctly classified for each given class. The off-diagonal elements show the number of data points that were incorrectly classified. The precision and false discovery rate for each class are also included. The two bottom-most rows show the recall and false-negative rate for each class. The prediction accuracy was 99.43%, and the confusion matrix

Optics EXPRESS

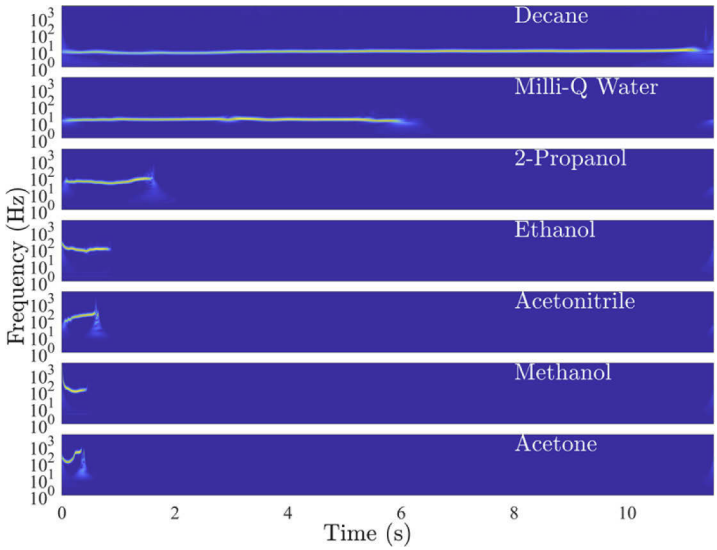

Fig. 4. Corresponding semi-log scalograms of the seven time-domain transient signals shown in Fig. 3 for seven different liquids. (Top) decane, milli-Q water, 2-propanol, ethanol, acetonitrile, methanol, and (bottom) acetone. The bright yellow regions indicate that at those time instances the presence of certain frequencies dominate the transient signal. This gives us an idea about the nature of the interference in the transient signal. When a test liquid has a high vapor pressure, the transient signal lasts for a shorter duration. We also see some boundary effects which occur in scalograms due to truncation and zero-padding of the signals, these manifest as shadows on the right corner of the scalogram.

showed that for 2-Propanol, 24 of 25 test signals were correctly classified, with only one of them wrongly classified into the class of Milli-Q Water.

The different ML models used were GoogLeNet [50], AlexNet [51], ResNet-18, ResNet-50 [52] and DenseNet-201 [53]. Note that all of the models used were pre-trained on ImageNet [47]. The results of the training are presented in Table 2. The DenseNet-201 and ResNet models showed the highest classification accuracies amongst the five models. In this study, the model ResNet-18 would be the optimal model choice as it performed very well with a comparably smaller number of parameters compared to four of the other models, and it was trained in less time than the other models that reported similar accuracies. The accuracy obtained for each model was more than 98% for the classification (identification) of the seven classes (seven pure liquids).

Table 2. The test Accuracy, the number of Parameters, and the Run-Time for the classification of pure liquids using different pre-trained CNN models.

Models	Accuracy (%)	Parameters (Millions)	Run-Time (mins)
GoogLeNet	98.86	7	11
AlexNet	98.29	61	4
DenseNet-201	99.43	20	186
ResNet-18	99.43	11.7	13
ResNet-50	99.43	25.6	61

Optics EXPRESS

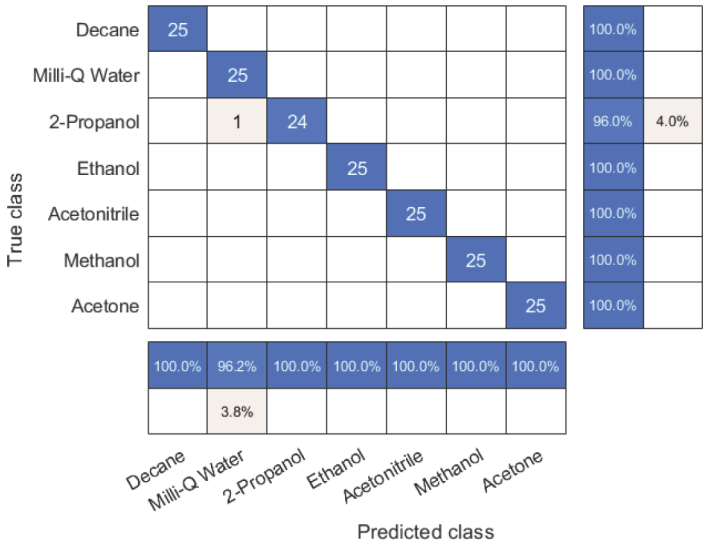

Fig. 5. Confusion matrix for the classification (identification) results of the pure liquids from the test composite dataset using the ResNet-18 model. For each class, recorded responses from 25 individual liquid droplet evaporation events were used. The confusion matrix displays the number of correct and incorrect predictions for each class (liquid) when using the ResNet-18 model.

3.2. *Evaporation events of ethanol-water binary mixtures*

In the second series of experiments, we demonstrate that the EFPI sensor was able to sense the evaporation events of liquid droplets of binary mixtures of ethanol and distilled water. The same experimental setup and procedure described in Section 2 were used. Distilled water and ethanol were mixed to formulate six different volume percent concentrations (vol/vol %) of ethanol in water solutions, including 100%, 80%, 60%, 40%, 20%, and 0%. Figure 6 shows the results of measured time-domain responses of the EFPI sensor for the six different binary mixtures within a transient time period of 3.5 seconds. Visual differences of the time-domain transient responses were observed, and 55 individual responses of liquid droplet evaporation experiments for each of the binary mixtures (a total of 330 responses for six different binary mixtures) were recorded. The time-domain responses were then processed using CWT and converted to semi-log scalograms, as shown in Fig. 7.

After the scalograms (matrices of size 157×164000) were converted into corresponding scalogram images, the five models were used for training the data samples using the Deep learning toolbox in MATLAB. The same algorithm described in Section 3.1 was employed. We again divided the composite dataset into 50% training, 25% validation, and 25% test datasets. The results from the classification (identification) of the six different concentrations of the ethanol-water binary mixtures using the GoogLeNet model are presented in the form of a confusion matrix in Fig. 8. Prediction accuracy of 100% was obtained. The results show that the EFPI sensor was able to identify the concentrations of ethanol in ethanol-water binary mixtures based on analyzing liquid mixture droplet evaporation transient events with the assistance of a machine learning model. We used different models of CNNs for training the same datasets, including GoogLeNet, AlexNet, ResNet-50, and DenseNet-201.

Table 3 shows the results for test Accuracy, Parameters, and Run-Time from the classification (identification) of the ethanol-water binary mixture composite dataset using different CNN models. The accuracy of prediction from all models was higher than 98%, with the highest accuracy

Optics EXPRESS

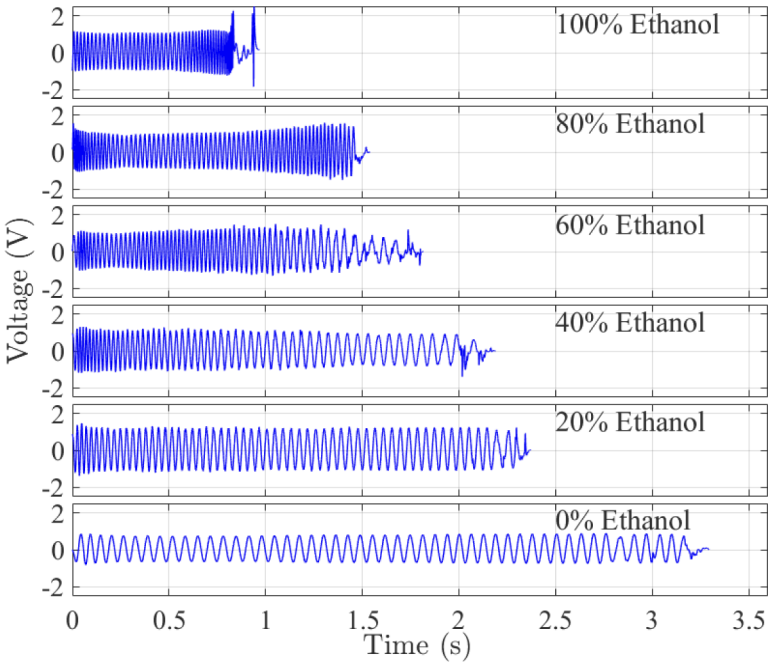

Fig. 6. Exemplary time-domain signals from the EFPI sensor for ethanol-water binary mixtures. Volume percent concentrations (vol/vol %) are included in the figure.

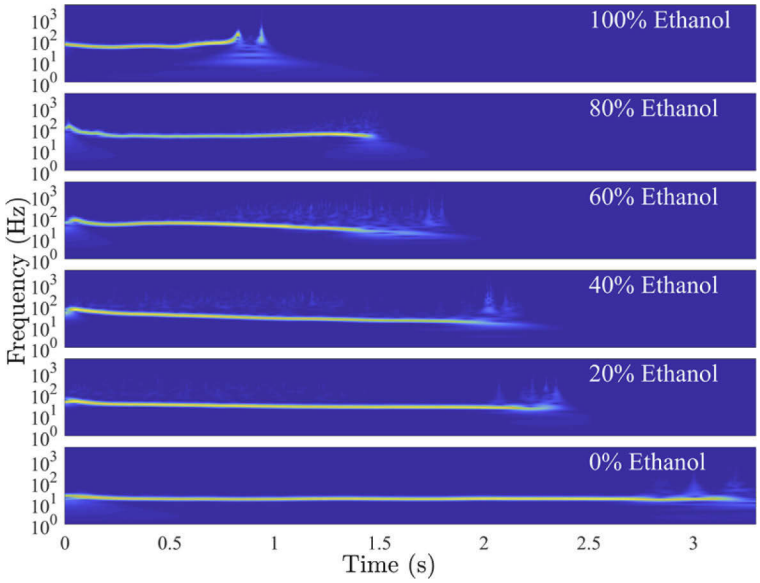

Fig. 7. Examples of semi-log scalograms for the ethanol-water binary mixtures for ethanol percent concentrations (vol/vol %) of 100%, 80%, 60%, 40%, 20%, and 0%. The semi-log scalograms shown correspond to the transient time-domain signals shown in Fig. 6. Volume percent concentrations (vol/vol %) are included in the figure. It was reported in [54] that as the percentage of ethanol in the binary mixture increased, the vapor pressure also increased in an almost linear fashion. As observed in Fig. 4, the duration of the transient signals increased with decreasing vapor pressure. The trend persists for binary mixtures as well.

Optics EXPRESS

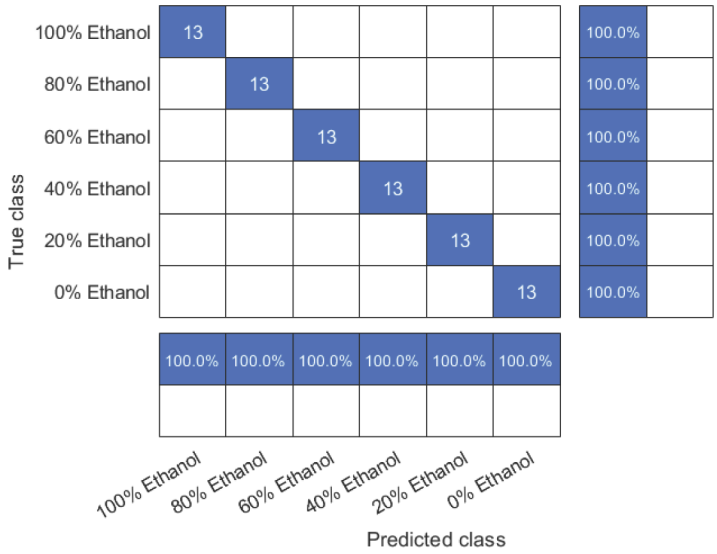

Fig. 8. Confusion matrix of the classification results using GoogLeNet model for the ethanol-water binary mixture test composite dataset.

being 100%. GoogLeNet was the optimal model choice when considering both training time and the number of parameters included in the model. Furthermore, we performed an additional experiment where different concentrations for ethanol-water binary mixtures (vol/vol %) of 2%, 4%, 6%, 8%, and 10%, were tested using the present sensor system. Noticeable differences were observed in the measured raw data, and different CNNs models were employed for data analysis. We found that the CNNs can still accurately identify the liquids with >96% accuracy, indicating a good concentration resolution of the present system. We are pursuing using surface-modified fiber optic sensor arrays to identify mixtures of three or more components.

Table 3. The test Accuracy, the number of Parameters, and the Run-Time for the classification of ethanol-water binary mixture dataset using different pre-trained CNN models.

Models	Accuracy (%)	Parameters (Millions)	Run-Time (mins)
GoogLeNet	100.0	7	5
AlexNet	98.7	61	2
DenseNet-201	98.7	20	83
ResNet-18	100.0	11.7	6
ResNet-50	98.7	25.6	21

All the models shown in Table 3 were comparable in performance (accuracy), considering that the composite test dataset was small (66 transient signals). Depending on the requirements of the final product or the end-user, other specific models may be more desirable. If the aim is to build a sensor prototype with the trained model retained in small local electronic media storage, then it would be desirable for the model to have a smaller number of parameters. In such a case, GoogLeNet or AlexNet may be used (there are other models, including Mobilenet [55] for such issues, which can also be considered). If the desire is to build a comprehensive model using a larger composite dataset, then considerations for both the training time and the number of parameters becomes essential, as smaller models may underfit the data, while larger models may overfit the data (models, which are optimized to give good performance with a smaller number of

Optics EXPRESS

parameters, are typically the best choice). Hence, in such cases, tried and tested models like the ResNet or the Efficientnet family of models may be used.

The present work demonstrates a simple sensing system for the classification (identification) of liquids and binary mixtures of liquids based on liquid droplet evaporation transient events and analyses employing machine learning techniques. The sensing system includes a single-mode fiber-optic cleaved tip sensor and a data acquisition unit. The fiber tip sensor is dipped and then pulled out of the liquid of interest; the cleaved endface of the optical fiber suspends the liquid pendant droplet. The liquid droplet forms an EFPI where the optical fiber-droplet interface and droplet-air interface serve as the two partial reflectors of the EFPI. As the liquid droplet evaporates, its length dimension diminishes, resulting in variations in the effective reflectance. As a result, the effective reflectance of the sensor changes quasi-periodically, metering the evaporation of the liquid droplet from the fiber endface. Time transient responses corresponding to the evaporation events of various liquids (i.e., pure liquids and ethanol-water binary mixtures) were recorded using single-wavelength probing light, resulting in evaporation time transient fingerprints of the liquids being studied. After a dataset of diverse liquids was acquired using the sensor, a continuous wavelet transform was employed to pre-process the time transient response for each liquid evaporation event and then convert the resultant temporal data structure to image data. Then, CNN models were used to learn a hierarchy of abstract features from the image datasets. The models underwent training, validation and were finally tested on test datasets. The outputs from the models yielded the classes (identities) that corresponded to the identified liquids, and performance metrics of the models were determined in terms of classification (identification) accuracies of the test datasets. The results showed that a simple fiber-optic tip sensing system combined with the assistance of CNN models could effectively predict the identities of different liquids and binary mixtures of liquids based on their evaporation transient fingerprints.

During the data collection process, because of variations in ambient temperature and human handling, the evaporation time transient events were not identical between any two measurements for the same liquid, especially the magnitude of the measured signal.

Variations of manually handling the optical fiber to perform the dipping experiments include the following:

a) Holding the optical fiber probe at a position of 5 ± 0.5 cm above the cleaved face.

b) Dipping and removing the fiber tip in the test liquid at a speed of 1 ± 0.1 cm/s and an angle of 90 ± 10 degrees

The variations in the experimental droplet evaporation transients caused by human handling as well as the variations of the laboratory temperature (23 ± 2 °C), fell well within the corresponding liquid classifications.

However, the machine learning models still performed very well and classified (identified) the liquids and binary mixtures of liquids with high accuracies. The outcomes of the experiments and the analyses lend credibility to our initial hypothesis that the information from droplet evaporation time transient events can be used to identify liquids and binary mixtures of liquids effectively.

4. Conclusions

We presented an extremely simple optical fiber tip sensor system and method for the identification of liquids. The method is based on liquid droplet evaporation time transient events that were identified using machine learning (ML) techniques. The machine learning-based analyses directly and efficiently extracted the relevant information embedded in the time domain evaporation time transient signals obtained from the EFPI sensor system. After proper training, the CNN models provided high prediction accuracies of greater than 98% for identifying seven different pure liquids and also for identifying ethanol-water binary mixtures of different concentrations.

Optics EXPRESS

This paper introduced a novel approach of combining a simple sensor system and method with machine learning techniques for smart sensing applications of pure liquids and mixtures of liquids. The sensor system has prominent merits such as high sensitivity, high resolution, high fidelity, and a rapid response time. The sensor system produces time-domain evaporation-based transient signals, which include rich information about pure liquids and mixtures of liquids. Unambiguous one-to-one mappings between evaporation curves (i.e., time-domain evaporation transient signals measured by the sensor) and the identities of liquids and binary liquid mixtures were achieved by utilizing machine-learning-based analyses to directly learn the features of the sensors' responses. The proposed sensor system and method, together with advanced data-driven analyses (i.e., machine learning), offer a complete, simple, and intelligent sensor system and method that can be expanded for developing a new generation of powerful sensor networks.

Acknowledgments. This research was supported by the Lightwave Technology Lab at the Missouri University of Science and Technology, Rolla, MO. J.H. is grateful for support from the Roy A. Wilkens Professorship Endowment. W.N. gratefully acknowledges a scholarship from the Royal Thai Government.

Disclosures. The authors declare no conflicts of interest.

Data availability. Data underlying the results presented in this paper are not publicly available at this time but may be obtained from the authors upon reasonable request.

References

1. D. Leopold, "Chapter 12 Intermolecular Forces : Liquids, Solids, and Phase Changes," pp. 2–4 (2019).
2. J. Arcamone, E. Dujardin, G. Rius, F. Pérez-Murano, and T. Ondarçuhu, "Evaporation of femtoliter sessile droplets monitored with nanomechanical mass sensors," J. Phys. Chem. B **111**(45), 13020–13027 (2007).
3. T. P. Bigioni, X. M. Lin, T. T. Nguyen, E. I. Corwin, T. A. Witten, and H. M. Jaeger, "Kinetically driven self assembly of highly ordered nanoparticle monolayers," Nat. Mater. **5**(4), 265–270 (2006).
4. T. Kawase, H. Sirringhaus, R. H. Friend, and T. Shimoda, "Inkjet printed via-hole interconnections and resistors for all-polymer transistor circuits," Adv. Mater. **13**(21), 1601–1605 (2001).
5. T. Ondarçuhu and C. Joachim, "Drawing a single nanofibre over hundreds of microns," Europhys. Lett. **42**(2), 215–220 (1998).
6. A. Gao, J. Liu, L. Ye, C. Schonecker, M. Kappl, H.-J. Butt, and W. Steffen, "Control of Droplet Evaporation on Oil-Coated Surfaces for the Synthesis of Asymmetric Supraparticles," Langmuir **35**(43), 14042–14048 (2019).
7. P. Innocenzi, L. Malfatti, S. Costacurta, T. Kidchob, M. Piccinini, and A. Marcelli, "Evaporation of ethanol and ethanol-water mixtures studied by time-resolved infrared spectroscopy," J. Phys. Chem. A **112**(29), 6512–6516 (2008).
8. E. Goto, K. Endo, A. Suzuki, Y. Fujikura, Y. Matsumoto, and K. Tsubota, "Tear evaporation dynamics in normal subjects and subjects with obstructive meibomian gland dysfunction," Invest. Ophthalmol. Vis. Sci. **44**(2), 533–539 (2003).
9. Y. Tang and Z. Wu, "Distributed long-gauge optical fiber sensors based self-sensing FRP bar for concrete structure," Sensors **16**(3), 286 (2016).
10. C. Zhu, Y. Chen, Y. Zhuang, Y. Du, R. E. Gerald II, Y. Tang, and J. Huang, "An optical interferometric triaxial displacement sensor for structural health monitoring: Characterization of sliding and debonding for a delamination process," Sensors **17**(11), 2696 (2017).
11. P. Roriz, O. Frazão, A. B. Lobo-Ribeiro, J. L. Santos, and J. A. Simões, "Review of fiber-optic pressure sensors for biomedical and biomechanical applications," J. Biomed. Opt. **18**(5), 050903 (2013).
12. Y. Huang, T. Wei, Z. Zhou, Y. Zhang, G. Chen, and H. Xiao, "An extrinsic Fabry-Perot interferometer-based large strain sensor with high resolution," Meas. Sci. Technol. **21**(10), 105308 (2010).
13. C. Zhu, Y. Chen, Y. Zhuang, G. Fang, X. Liu, and J. Huang, "Optical Interferometric Pressure Sensor Based on a Buckled Beam with Low-Temperature Cross-Sensitivity," IEEE Trans. Instrum. Meas. **67**(4), 950–955 (2018).
14. Y. Zhao, X. G. Li, L. Cai, and Y. N. Zhang, "Measurement of RI and Temperature Using Composite Interferometer with Hollow-Core Fiber and Photonic Crystal Fiber," IEEE Trans. Instrum. Meas. **65**(11), 2631–2636 (2016).
15. Y. B. Yang, D. N. Wang, and B. Xu, "Optical Fiber Pressure Sensor Based on SMF-Capillary Structure," *Asia Commun. Photonics Conf. ACP*, vol. 2018-Octob, pp. 1–3 (2018).
16. J. Huang, X. Lan, M. Luo, and H. Xiao, "Spatially continuous distributed fiber optic sensing using optical carrier based microwave interferometry," Opt. Express **22**(15), 18757 (2014).
17. C. Zhu, Y. Chen, Y. Du, Y. Zhuang, F. Liu, R. E. Gerald II, and J. Huang, "A Displacement Sensor with Centimeter Dynamic Range and Submicrometer Resolution Based on an Optical Interferometer," IEEE Sens. J. **17**(17), 1 (2017).
18. Z. Chen, L. Yuan, G. Hefferman, and T. Wei, "Ultraweak intrinsic Fabry–Perot cavity array for distributed sensing," Opt. Lett. **40**(3), 320 (2015).
19. J. Chen, B. Liu, and H. Zhang, "Review of fiber Bragg grating sensor technology," Front. Optoelectron. China **4**(2), 204–212 (2011).

Optics EXPRESS

20. V. M. N. Passaro, A. Cuccovillo, L. Vaiani, M. De Carlo, and C. E. Campanella, "Gyroscope technology and applications: A review in the industrial perspective," Sensors **17**(10), 2284 (2017).
21. B. H. Lee, Y. H. Kim, K. S. Park, J. B. Eom, M. J. Kim, B. S. Rho, and H. Y. Choi, "Interferometric fiber optic sensors," Sensors **12**(3), 2467–2486 (2012).
22. E. Preter, B. Preloznik, V. Artel, C. N. Sukenik, D. Donlagic, and A. Zadok, "Monitoring the evaporation of fluids from fiber-optic micro-cell cavities," Sensors **13**(11), 15261–15273 (2013).
23. V. Salazar-Haro, V. Márquez-Cruz, and J. Hernández-Cordero, "Liquids analysis using back reflection single-mode fiber sensors," *22nd Congr. Int. Comm. Opt. Light Dev. World*, vol. 8011, p. 80114W (2011).
24. J. P. Moura, H. Baierl, J.-L. Auguste, R. Jamier, P. Roy, J. L. Santos, and O. Frazão, "Evaporation of fluids in suspended-core fibres," *2014 3rd Mediterr. Photonics Conf. MePhoCo 2014*, pp. 2–4 (2014).
25. Y. Du, Y. Chen, C. Zhu, Y. Zhuang, and J. Huang, "An embeddable optical strain gauge based on a buckled beam," Rev. Sci. Instrum. **88**(11), 115002 (2017).
26. Y. Zhuang, Y. Chen, C. Zhu, R. E. Gerald II, and J. Huang, "Probing changes in tilt angle with 20 nanoradian resolution using an extrinsic Fabry-Perot interferometer-based optical fiber inclinometer," Opt. Express **26**(3), 2546 (2018).
27. O. R. Lim, H. T. Cho, G. S. Seo, M. K. Kwon, and T. J. Ahn, "Evaporation Rate Sensor of Liquids Using a Simple Fiber Optic Configuration," *2018 Conf. Lasers Electro-Optics Pacific Rim, CLEO-PR 2018*, vol. 2, pp. 1–2 (2018).
28. E. Preter, M. Katzman, Z. Oren, M. Ronen, D. Gerber, and A. Zadok, "Fiber-optic evaporation sensing: Monitoring environmental conditions and urinalysis," J. Lightwave Technol. **34**(19), 4486–4492 (2016).
29. O. R. Lim and T. J. Ahn, "Fiber-optic measurement of liquid evaporation dynamics using signal processing," J. Lightwave Technol. **37**(19), 4967–4975 (2019).
30. Y. Guo, N. An, K. Guo, Y. Li, Y. Liang, C. Wu, Y. Wang, J. He, Y. Wang, T. Tan, Y. Rao, and B. Yao, "Gas detection in a graphene based dual-mode fiber laser microcavity," Sensors and Actuators B: Chemical **348**(7), 130694 (2021).
31. Y. Lecun, Y. Bengio, and G. Hinton, "Deep learning," Nature **521**(7553), 436–444 (2015).
32. Z. Qibin and Z. Liqing, "ECG feature extraction and classification using wavelet transform and support vector machines," *Proc. 2005 Int. Conf. Neural Networks Brain Proceedings, ICNNB'05*, vol. 2, pp. 1089–1092 (2005).
33. B. J. Erickson, P. Korfiatis, Z. Akkus, and T. L. Kline, "Machine learning for medical imaging," Radiographics **37**(2), 505–515 (2017).
34. D. J. Lary, A. H. Alavi, A. H. Gandomi, and A. L. Walker, "Machine learning in geosciences and remote sensing," Geosci. Front. **7**(1), 3–10 (2016).
35. A. E. Maxwell, T. A. Warner, and F. Fang, "Implementation of machine-learning classification in remote sensing: An applied review," Int. J. Remote Sens. **39**(9), 2784–2817 (2018).
36. Z. Peng, J. Jian, H. Wen, A. Gribok, M. Wang, H. Liq, S. Huang, Z Mao, and K. P. Chen, "Distributed fiber sensor and machine learning data analytics for pipeline protection against extrinsic intrusions and intrinsic corrosions," Opt. Express **28**(19), 27277 (2020).
37. T. Tan, C. Peng, Z. Yuan, X. Xie, H. Liu, Z. Xie, S. Huang, Y. Rao, and B. Yao, "Predicting kerr soliton combs in microresonators via deep neural networks," J. Lightwave Technol. **38**(23), 6591–6599 (2020).
38. C. Zhu, R. E. Gerald II, Y. Chen, and J. Huang, "One-dimensional sensor learns to sense three-dimensional space," Opt. Express **28**(13), 19374 (2020).
39. C. Zhu, Y. Chen, R. E. Gerald, and J. Huang, "Probing Changes in Pressure with Subpascal Resolution Using an Optical Fiber Fabry-Perot Interferometer," IEEE Trans. Instrum. Meas. **69**(9), 6556–6563 (2020).
40. Y. LeCun, L. Bottou, Y. Bengio, and P. Haffner, "Gradient-based learning applied to document recognition," Proc. IEEE **86**, 2278–2324 (1998).
41. Z.-W. Yuan and J. Zhang, "Feature extraction and image retrieval based on AlexNet," *Eighth Int. Conf. Digit. Image Process. (ICDIP 2016)*, vol. 10033, no. Icdip 2016, p. 100330E (2016).
42. V. Giurgiutiu, "Chapter 14 - Signal Processing and Pattern Recognition for Structural Health Monitoring with PWAS Transducers," in *Structural Health Monitoring with Piezoelectric Wafer Active Sensors (Second Edition)*, 2nd Edi., V. Giurgiutiu, Ed. Oxford: Academic Press, (2014, pp. 807–862.
43. M. Stéphane, "CHAPTER 4 - Time Meets Frequency," in *A Wavelet Tour of Signal Processing (Third Edition)*, 3rd Edit., M. Stéphane, Ed. Academic Press: Boston, (2009, pp. 89–153.
44. J. M. Lilly, "Element analysis: A wavelet-based method for analysing time-localized events in noisy time series," Proc. R. Soc. A Math. Phys. Eng. Sci. **473**(2200), 20160776 (2017).
45. E. Preter, R. A. Katims, V. Artel, C. N. Sukenik, D. Donlagic, and A. Zadok, "Monitoring and analysis of pendant droplets evaporation using bare and monolayer-coated optical fiber facets," Opt. Mater. Express **4**(5), 903 (2014).
46. J. Tian, Z. Lu, M. Quan, Y. Jiao, and Y. Yao, "Fast response Fabry–Perot interferometer microfluidic refractive index fiber sensor based on concave-core photonic crystal fiber," Opt. Express **24**(18), 20132 (2016).
47. J. Deng, W. Dong, R. Socher, L.- J. Li, K. Li, and L. Fei-Fei, "ImageNet: A large-scale hierarchical image database," *2009 IEEE Conference on Computer Vision and Pattern Recognition* (2009), pp. 248–255.
48. X. Jiang, B. Hu, S. C. Satapathy, S. H. Wang, and Y. D. Zhang, "Fingerspelling Identification for Chinese Sign Language via AlexNet-Based Transfer Learning and Adam Optimizer," Sci. Program. **2020**, 3291426 (2020).
49. S. Bock and M. Weis, "A Proof of Local Convergence for the Adam Optimizer," *2019 International Joint Conference on Neural Networks (IJCNN)* (2019).

Optics EXPRESS

50. C. Szegedy, W. Liu, Y. Jia, P. Sermanet, S. Reed, D. Anguelov, D. Erhan, V. Vanhoucke, and A. Rabinovich, "Going deeper with convolutions," *Proc. IEEE Comput. Soc. Conf. Comput. Vis. Pattern Recognit.*, vol. 07-12-June, pp. 1–9 (2015).
51. A. Krizhevsky, I. Sutskever, and G. E. Hinton, "ImageNet Classification with Deep Convolutional Neural Networks," *Advances in Neural Information Processing Systems* 25, 1097–1105 (2012).
52. K. He, X. Zhang, S. Ren, and J. Sun, "Deep residual learning for image recognition," *Proc. IEEE Comput. Soc. Conf. Comput. Vis. Pattern Recognit.*, vol. 2016-Decem, pp. 770–778, 2016.
53. J. Zhang, C. Lu, X. Li, H. J. Kim, and J. Wang, "A full convolutional network based on DenseNet for remote sensing scene classification," Math. Biosci. Eng. **16**(5), 3345–3367 (2019).
54. C. Liu, E. Bonaccurso, and H. J. Butt, "Evaporation of sessile water/ethanol drops in a controlled environment," Phys. Chem. Chem. Phys. **10**(47), 7150–7157 (2008).
55. A. G. Howard, M. Zhu, B. Chen, D. Kalenichenko, W. Wang, T. Weyand, M. Andreetto, and H. Adam, "MobileNets: Efficient Convolutional Neural Networks for Mobile Vision Applications," arXiv:1704.04861 [cs.CV] (2017).